



A model for rubber elasticity

W. E. VanArsdale¹

Received: 13 February 2020 / Revised: 28 June 2020 / Accepted: 8 July 2020 / Published online: 17 October 2020
© Springer-Verlag GmbH Germany, part of Springer Nature 2020

Abstract

A constitutive equation for rubber-like materials is developed using the left stretch tensor. This process starts with a model for hyperelastic solids based on a separable energy function. This model accurately fits extensional data for vulcanized natural rubber until the onset of hysteresis at intermediate strains. Better predictions outside the hyperelastic range are obtained by directly modifying this constitutive equation to describe limited extensibility. The resulting model accurately fits biaxial, planar, and uniaxial extension data for a variety of rubber-like materials using three constants. This model also predicts simple shear results derived from planar extension data and characterizes inflation of spherical membranes for elastomers and soft tissue. A final modification accurately describes hardening associated with crystallization at large tensile strains.

Keywords Finite strain · Hysteresis · Left stretch tensor · Rubber material · Soft tissue

Introduction

Vulcanized rubber is an isotropic material consisting of crosslinked polymers. This material is typically modeled as an incompressible, hyperelastic solid, where deformation is characterized by the *left Cauchy–Green tensor* $\mathbf{B} = \mathbf{F}\mathbf{F}^T$ defined in terms of the *deformation gradient* \mathbf{F} (Gurtin 1981 p. 46). This objective tensor is usually assumed to be consistent with the *isochoric constraint* $\det(\mathbf{B}) = 1$. However, applying tensile stress to vulcanized rubber causes volume to increase until *strain-induced crystallization* results in a decrease at large strains (Treloar 2009 pp. 295, 20–23). Filled and unfilled natural rubber also exhibit *hysteresis* at intermediate strains (Omnès et al. 2008, Treloar 2009 pp. 87, 89, 92), implying work in a closed cycle of deformation. While this behavior is *inconsistent* with predictions for hyperelastic solids (Gurtin 1981 p. 190), these models are still used to fit extensional data at large strains.

Constitutive equations for *hyperelastic* solids derive stress from an *energy function*. Rivlin (1948) developed models for rubber-like materials based on functions of the invariants $\text{tr}(\mathbf{B})$ and $\text{tr}(\mathbf{B}^{-1})$. For example, the function

$$w = C_1[\text{tr}(\mathbf{B})-3] + C_2[\text{tr}(\mathbf{B}^{-1})-3] \quad (1)$$

involving constants C_1 and C_2 determines *Cauchy stress*

$$\mathbf{T} = -p\mathbf{I} + 2C_1\mathbf{B} - 2C_2\mathbf{B}^{-1} \quad (2)$$

to within an unspecified *pressure* p associated with the constraint $\det(\mathbf{B}) = 1$. While many models use this approach (Hoss and Marczak 2010), most energy functions depend only on the invariant $\text{tr}(\mathbf{B})$. For example, Treloar (1943) used network theory with a Gaussian distribution function to derive the *neo-Hookean model*

$$\mathbf{T} = -p\mathbf{I} + 2C_1\mathbf{B}, \quad (3)$$

where \mathbf{I} is the *identity tensor*. Theories for non-Gaussian networks of flexible chains lead to similar models (Arruda and Boyce 1993; Horgan et al. 2004), where C_1 becomes a function of $\text{tr}(\mathbf{B})$.

Unfortunately, models based on energy functions involving $\text{tr}(\mathbf{B})$ and $\text{tr}(\mathbf{B}^{-1})$ have generally failed to describe data for rubber-like materials as summarized by Destrade et al. (2017).

“Following World War II, a huge research effort was launched to find an explicit strain-energy function able to describe accurately the experimental data obtained from the testing of natural and synthetic rubbers. However, in spite of decades of intensive work in that area, to this day there is still no effective model able to

✉ W. E. VanArsdale

¹ Colorado Springs, USA

perform this task in a satisfying and universal way. ... Here, a satisfactory model is defined as a model able to describe the experimental data first of all from a qualitative point of view and then from a quantitative point with acceptable relative errors of prediction with respect to the data.”

Perhaps using models for hyperelastic materials outside their range of validity contributed to this lack of success.

Varga (1966) suggested an alternate approach to modeling rubber-like materials using the *left stretch tensor V*. This symmetric tensor and the *material rotation R* determine a *polar decomposition F = VR* of the deformation gradient (Richter 1952; Gurtin 1981 p. 46). Varga’s *linear principal stress–strain model* assumes stress is proportional to the objective *strain tensor V – I*, which is also used here to describe strain. This constitutive equation is derivable from an energy function involving $\text{tr}(\mathbf{V})$. Varga’s approach, like the neo-Hookean model (3), accurately describes Treloar’s (1944) extensional data for vulcanized natural rubber out to 50–70% strain depending on the type of deformation (Ogden 1972a, Fig. 1). Even with this limited range, Varga (1966) obtains good results for several problems involving finite deformation.

Other models for hyperelastic materials specify the energy function in terms of positive *principal stretches* ($\lambda_1, \lambda_2, \lambda_3$) associated with a spectral decomposition of \mathbf{V} (Gurtin 1981 pp. 11–12). For example, Mooney (1940) assumed shear stress and strain are proportional in simple shear to develop the energy function (1) in terms of ($\lambda_1, \lambda_2, \lambda_3$). Ogden (1972a, 1984 p. 494) later fit Treloar’s (1944) extensional data out to 600% strain as well as biaxial data obtained by Jones and Treloar (1975) using a function involving six constants

$$w = \sum_{i=1}^3 \mu_i (\lambda_1^{\alpha_i} + \lambda_2^{\alpha_i} + \lambda_3^{\alpha_i} - 3), \tag{4}$$

where exponents ($\alpha_1, \alpha_2, \alpha_3$) can take non-integer values. Varga’s model is a special case of (4) with constants μ_1 and $\alpha_1 = 1$, while the function (1) also has this form using expressions $\text{tr}(\mathbf{B}) = \lambda_1^2 + \lambda_2^2 + \lambda_3^2$ and $\text{tr}(\mathbf{B}^{-1}) = \lambda_1^{-2} + \lambda_2^{-2} + \lambda_3^{-2}$ for the invariants.

Varga (1966 p. 88), Ogden (1972a), and Treloar (2009 p. 215) all reject Rivlin’s (1948) requirement that strain energy depends *only* on squared principal stretches. Specifically, Treloar (2009 p. 233) states that “...the restriction of the strain energy function to even powers of extension ratios have no necessary basis in physical reality.” However, the function (1) can be expressed in the *separable form*

$$w = W(\lambda_1) + W(\lambda_2) + W(\lambda_3) \tag{5}$$

suggested by Valanis and Landel (1967). An accurate description of biaxial data apparently requires an energy function to be consistent with this form, like Ogden’s model (4). While

this constraint is not sufficient, models based on non-separable energy functions generally fail to fit and superpose biaxial data. See Treloar (2009 pp. 236–251) and Ogden (1984 pp. 488–501) for further discussion of separable energy functions and their role in describing hyperelastic materials.

General constitutive equations for isotropic elastic solids use the deformation tensor \mathbf{B} or the stretch tensor \mathbf{V} to describe large strains (Gurtin 1981 pp. 170–171; Truesdell and Noll 1992 p. 140). Models based on \mathbf{B} can easily be converted to a function of \mathbf{V} since $\mathbf{B} = \mathbf{V}^2$. For example, the Mooney–Rivlin model (2) is expressed in terms of the left stretch tensor in Appendix 1. However, converting a simple model like Varga’s to an isotropic function of \mathbf{B} results in a very complicated expression requiring the positive root of a quartic equation (see Appendix 1). This asymmetry suggests that \mathbf{V} may be a better variable for modeling elastic materials, especially since Varga’s model provides an accurate description of Treloar’s (1944) extensional data for relatively small strains. A model for rubber elasticity is developed in the next section using this approach.

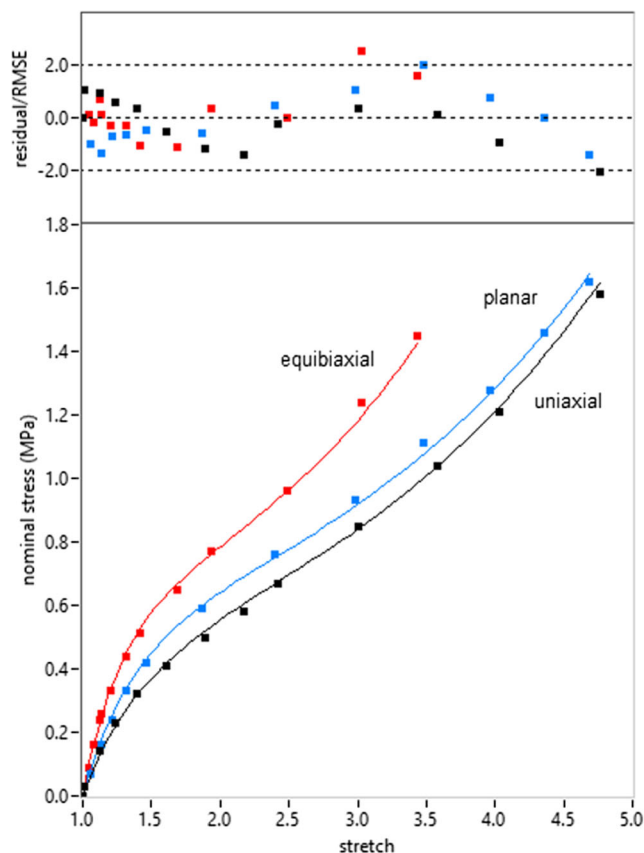


Fig. 1 A fit of extensional data (Treloar 1944) for $|\mathbf{V}| < 3.5$ using Eq. (7), where coefficients $m_1 = 0.740$ MPa and $m_2 = 0.0261$ MPa determine all curves with a *goodness of fit* $R^2 = 0.9988$, *relative error* $E = 4.6\%$, and *sum of squared error* $SSE = 0.010$ (MPa)². *Residuals* are differences between data and fitted values. These differences are normalized by the *root mean squared error* $RMSE = 0.0168$ MPa, which is about 1% of *full scale* for 39 data points shown in the figure. See Appendix 4 for additional information about determining model coefficients and statistics

Elastic solids

A constitutive equation for isotropic elastic solids (see Appendix 1) can be expressed as

$$\mathbf{T} = -p\mathbf{I} + M_1\mathbf{V} + M_2\mathbf{V}^2 \tag{6}$$

in terms of the left stretch tensor \mathbf{V} , an unspecified pressure p and scalar coefficients M_1 and M_2 . These moduli may depend on *moment invariants* $I_1 = \text{tr}(\mathbf{V})$ and $I_2 = \text{tr}(\mathbf{V}^2)$, while the remaining invariant $J = \det(\mathbf{V}) = 1$ is constant for incompressible materials. This solid has a fixed reference configuration, where $\mathbf{V} = \mathbf{I}$ and the Cauchy stress \mathbf{T} reduces to a pressure determined by boundary conditions. For small deformations from this reference state ($\mathbf{F} \approx \mathbf{I}$), the left stretch tensor and moment invariants become

$$\mathbf{V} \approx \mathbf{I} + \boldsymbol{\varepsilon}, \text{tr}(\mathbf{V}) \approx 3 + \text{tr}(\boldsymbol{\varepsilon}), \text{tr}(\mathbf{V}^2) \approx 3 + 2\text{tr}(\boldsymbol{\varepsilon})$$

to within products of the non-objective *Cauchy strain* $\boldsymbol{\varepsilon} = [\text{grad}(\mathbf{u}) + \text{grad}(\mathbf{u})^T]/2$, where the *displacement gradient* can be expressed as $\mathbf{F} - \mathbf{I}$ (Gurtin 1981 p. 42). The resulting approximation

$$\mathbf{T} \approx -p\mathbf{I} + 2\mu\boldsymbol{\varepsilon}$$

determines stress for an incompressible *linear elastic solid* with a positive *shear modulus* $\mu = M_1/2 + M_2$, where material parameters are evaluated at $I_1 = 3$ and $I_2 = 3$.

Coefficients M_1 and M_2 in Eq. (6) are usually specified by fitting extensional data like Treloar (1944). Attempts involving powers of $I_1/3$ and $I_2/3$ suggest the expressions $M_1 = m_1$ and $M_2 = m_2 I_2/3$, where constants m_1 and m_2 satisfy the constraint $\mu = m_1/2 + m_2 > 0$ to ensure a positive shear modulus. The first term after pressure in the resulting constitutive equation

$$\mathbf{T} = -p\mathbf{I} + m_1\mathbf{V} + m_2 I_2 \mathbf{V}^2/3 \tag{7}$$

is essentially Varga’s model, while the last term with $\mathbf{V}^2 = \mathbf{B}$ and $I_2 = \text{tr}(\mathbf{B})$ is a variant of the neo-Hookean model (3). This term also appears in models derived from an energy function involving $\text{tr}(\mathbf{B})^2$ as listed in Treloar (2009 p. 231) and Hoss and Marczak (2010). This result suggests that the constitutive eq. (7) can also be derived from an energy function.

An incompressible elastic solid (6) is *hyperelastic* (see Appendix 2) if Cauchy stress can be expressed as

$$\mathbf{T} = -p\mathbf{I} + \frac{\partial w}{\partial I_1} \mathbf{V} + 2 \frac{\partial w}{\partial I_2} \mathbf{V}^2 \tag{8}$$

in terms of a scalar function $w(I_1, I_2)$ of invariants $I_1 = \text{tr}(\mathbf{V})$ and $I_2 = \text{tr}(\mathbf{V}^2)$. The constitutive model (7) is readily obtained using the function

$$w(I_1, I_2) = m_1(I_1 - 3) + m_2(I_2^2 - 9)/12, \tag{9}$$

which is *convex* if $m_2 \geq 0$. The moment invariants become $I_1 = \lambda_1 + \lambda_2 + \lambda_3$ and $I_2 = \lambda_1^2 + \lambda_2^2 + \lambda_3^2$ in terms of principal

stretches consistent with the constraint $J = \lambda_1 \lambda_2 \lambda_3 = 1$. Substituting these results into (9) gives an alternate form of the energy function

$$\begin{aligned} \widehat{w}(\lambda_1, \lambda_2, \lambda_3) = & m_1(\lambda_1, \lambda_2, \lambda_3 - 3) \\ & + m_2(\lambda_1^4 + \lambda_2^4 + \lambda_3^4 + 2\lambda_1^{-2} + 2\lambda_2^{-2} + 2\lambda_3^{-2} - 9)/12 \end{aligned} \tag{10}$$

in terms of stretches. This expression is a special case of the energy function (4) with constants ($\mu_1 = m_1, \mu_2 = m_2/12, \mu_3 = m_2/6, \alpha_1 = 1, \alpha_2 = 4, \alpha_3 = -2$). Ogden (1984 pp. 495, 498) used similar exponent values ($\alpha_1 = 1.3, \alpha_2 = 5, \alpha_3 = -2$) and ($\alpha_1 = 1.3, \alpha_2 = 4, \alpha_3 = -2$) to fit extensional data by Treloar (1944) and Jones and Treloar (1975). The function

$$W(\lambda) = m_1(\lambda - 1) + m_2(\lambda^4 + 2\lambda^{-2} - 3)/12$$

can be used to express (10) in the separable form (5), where $dW/d\lambda = m_1 + m_2(\lambda^3 - \lambda^{-3})/3 = \widehat{W}(\lambda)$ determines a shift factor $\lambda \widehat{W}(\lambda)$ for superposing biaxial data (Treloar 2009 pp. 241).

Treloar (1944) performed experiments on vulcanized natural rubber in equibiaxial, planar, and uniaxial extension. These results are usually expressed in terms of the *nominal* or *first Piola–Kirchhoff stress* (Gurtin 1981 p. 178)

$$\mathbf{P} = \det(\mathbf{F}) \mathbf{T} \mathbf{F}^{-T},$$

where $\det(\mathbf{F}) = 1$ for incompressible materials. Expressions for

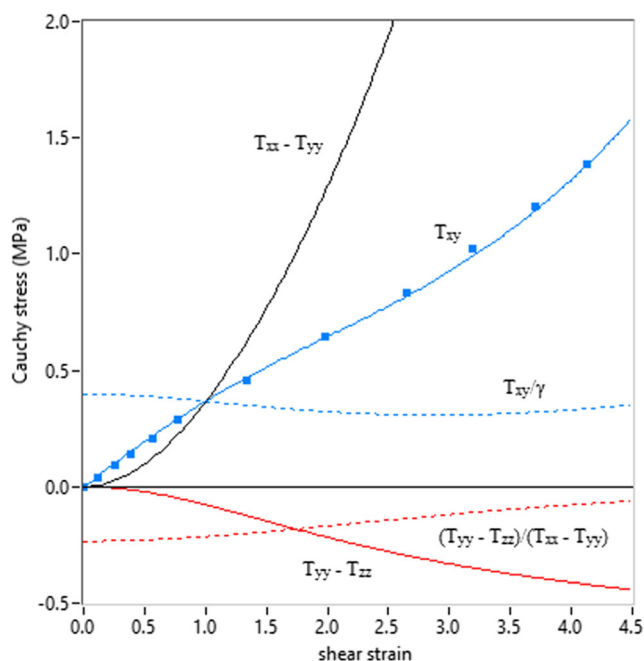


Fig. 2 Shear stress values derived from Treloar’s planar extension data shown in Fig. 1 using the equivalence relations (11). Curves are predictions of Eq. (7) using coefficients from Fig. 1 with correlation $R^2 = 0.9990$ to derived data. The deviation from predicted values $\text{RMSE} = 0.0167$ MPa is about 1% of full scale for derived data shown in the figure

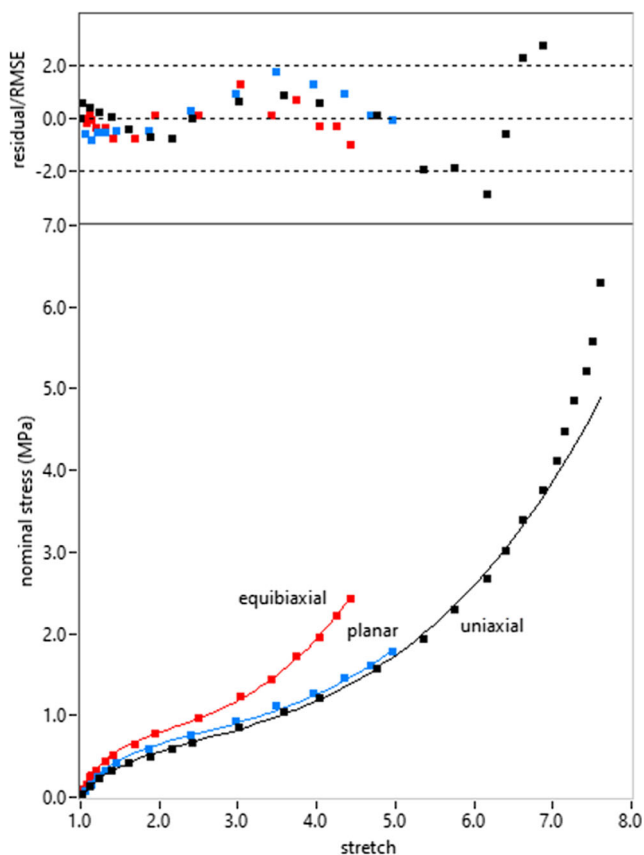


Fig. 3 A fit of extensional data (Treloar 1944) to $|V|=5$ using Eq. (12), where coefficients $m_1 = 0.762$ MPa, $m_2 = 0.0216$ MPa, and $\beta = 0.0446$ determine curves with correlation $R^2 = 0.9990$, relative error $E = 5.2\%$, and $SSE = 0.045$ (MPa)². The distribution of error is normalized by $RMSE = 0.0309$ MPa, which is about 0.8% of full scale for 50 data points ($\lambda < 7$). The uniaxial curve is extrapolated beyond fitted data to show model deviation at large strains. This fit is visually similar to results by Ogden 1972a, Fig. 4) using the six-constant energy function (4)

the nominal stress component P_{xx} given in Appendix 3 are fit to Treloar’s data (see Steimann et al. 2012) using a method described in Appendix 4. These comparisons are limited to a range consistent with an upper bound on the stretch magnitude $|V|$, where $|V|^2 = I_2/2 \geq 3/2$. For example, the term involving m_1 fits data ($R^2 = 0.9961$) for $1.225 \leq |V| < 1.7$, similar to comparisons by Ogden 1972a, Fig. 1). The term involving m_2 becomes necessary outside this range, resulting in a better fit ($R^2 = 0.9988$) out to $|V| = 3.5$ as shown in Fig. 1. This figure also shows the distribution of error using normalized residuals (see Appendix 4). While this approach can fit data ($R^2 = 0.9968$) out to $|V| = 5$, the root mean squared error increases significantly ($0.0168 \rightarrow 0.0583$ MPa). This increased error and a poorer fit suggest different material behavior for $|V| > 3.5$. Nah et al. (2010) question the value of modeling vulcanized natural rubber as hyperelastic for strains greater than 300%.

Simple shear results in Appendix 3 accurately predict derived data shown in Fig. 2. Here, shear stress T_{xy} is obtained as a function of shear strain γ from planar extension measurements in Fig. 1 using the equivalence relations

$$\gamma = \lambda - \lambda^{-1}, T_{xy} = P_{xx} / (1 + \lambda^{-2}) \tag{11}$$

given by Treloar (2009 pp. 84, 93 with a sign correction on the last exponent). This agreement is not surprising since the constitutive model (7) fits planar extension data in Fig. 1 and identically satisfies (11). The ratio T_{xy}/γ is relatively constant in Fig. 2, decreasing by less than 20% from an initial value $\mu = m_1/2 + m_2 = 0.396$ MPa. Destrade et al. (2017) obtain 8% to 24% higher estimates for μ by fitting models only to Treloar’s uniaxial data (see Appendix 5).

As expected, model (7) is consistent with the universal result (Gurtin 1981 p. 177)

$$T_{xx} - T_{yy} = \gamma T_{xy}$$

relating primary normal stress difference $N_1 = T_{xx} - T_{yy}$ to shear stress T_{xy} for all elastic solids. This result and (11) suggest another equivalence relation $N_1 = P_{xx}(\lambda - \lambda^{-1})/(1 + \lambda^{-2})$ with planar extension data. While $N_1 \geq 0$, the secondary normal stress difference $N_2 = T_{yy} - T_{zz}$ is typically negative with $-m_1 \leq N_2 \leq 0$ for $m_1 > 0$. In this case, the ratio N_2/N_1

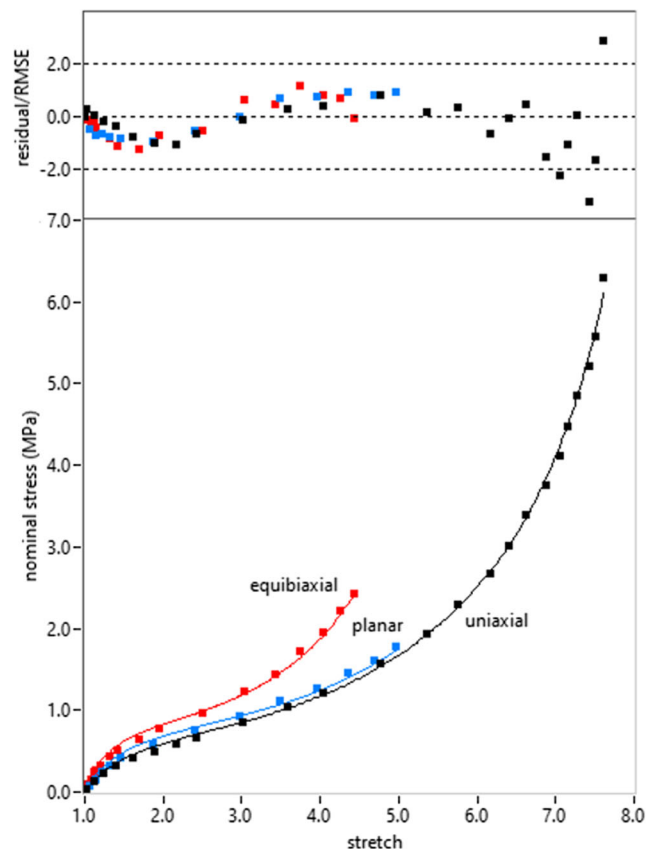


Fig. 4 A fit of extensional data (Treloar 1944) for a vulcanized natural rubber using the model (14), where coefficients $m_1 = 0.824$ MPa, $m_2 = 0.0191$ MPa, $\beta = 0.0390$, and $\alpha = 4.04E-5$ determine curves with correlation $R^2 = 0.9989$, relative error $E = 11.9\%$, and $SSE = 0.15$ (MPa)². The distribution of error is normalized by $RMSE = 0.0530$ MPa, which is about 0.8% of full scale for 56 data points shown in the figure

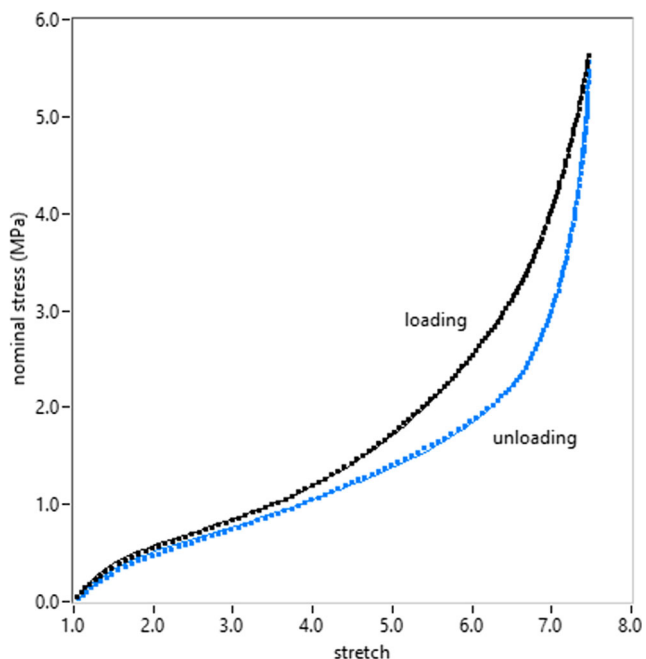
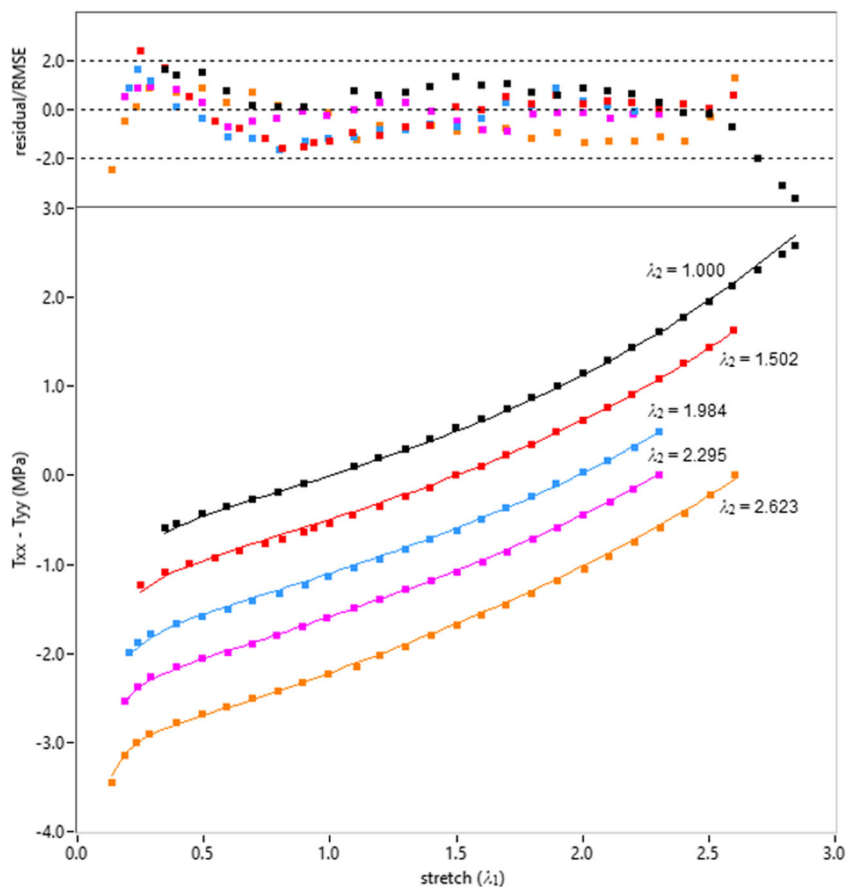


Fig. 5 Fits of uniaxial data (Treloar 2009 p. 87) for a vulcanized natural rubber using model (14), where points are obtained from curves in the reference. Coefficients $m_1 = 0.785$ MPa, $m_2 = 0.0225$ MPa, $\beta = 0.0176$, and $\alpha = 3.66E-8$ fit loading data with correlation $R^2 = 0.9999$ and shear modulus $\mu = 0.415$ MPa. Coefficients $m_1 = 0.586$ MPa, $m_2 = 0.0542$ MPa, $\beta = -0.599$, and $\alpha = -1.02E-8$ fit unloading data with correlation $R^2 = 0.9989$ and shear modulus $\mu = 0.347$ MPa

Fig. 6 A fit of biaxial data (Jones and Treloar 1975) for a vulcanized natural rubber using Eq. (12), where coefficients $m_1 = 0.722$ MPa, $m_2 = 0.0901$ MPa, and $\beta = -0.358$ determine curves with correlation $R^2 = 0.9995$, relative error $E = 9.4\%$, and $SSE = 0.11$ (MPa)². The distribution of error is normalized by $RMSE = 0.0302$ MPa, which is about 0.5% of full scale for 125 data points shown in the figure. This fit compares well to correlations based on the energy function (4) using twice as many constants (Ogden 1984 p. 494; Ogden et al. 2004, Fig. 11)



increases from an initial value $-m_1/8\mu = -0.234$ to zero like steady shear data for polystyrene solutions (Hua et al. 1999). Tractions associated with T_{yy} are negative if $m_1 > 0$, which implies axial elongation in torsion observed by Poynting (1913) for twisted rubber cords. Similar results are obtained for silicone rubber in Appendix 5, while a negative Poynting effect involving axial contraction ($m_1 < 0$) is predicted for porcine liver tissue. Models derived from an energy function depending only on the invariant $\text{tr}(\mathbf{B}) = \text{tr}(\mathbf{V}^2)$ predict no Poynting effect (Horgan and Smayda 2012).

In Treloar’s various extensional tests, hysteresis appears during unloading (Treloar 2009 pp. 87, 89, 92) at some point in the range $3.1 < |\mathbf{V}| < 3.6$. While the constitutive Eq. (7) does not predict this behavior, correlation with Treloar’s data for $|\mathbf{V}| > 3.5$ can be improved by simply replacing m_2 with $m_2/[1 - \beta(I_1 - 3)]$. Gent (1996) suggested a similar model for hyperelastic solids using a dimensionless parameter β^{-1} and the invariant $\text{tr}(\mathbf{B}) = \text{tr}(\mathbf{V}^2)$ instead of $I_1 = \text{tr}(\mathbf{V})$. Here, the resulting constitutive equation

$$\mathbf{T} = -p\mathbf{I} = m_1\mathbf{V} + m_2I_2\mathbf{V}^2/3[1-\beta(I_1-3)] \tag{12}$$

reduces to (7) for $\beta = 0$. If $\beta > 0$, stress becomes unbounded for $I_1 = 3 + \beta^{-1}$. This *limited extensibility* is associated with crosslinked polymers being stretched to their full extent. This limit should decrease at larger strain as more chains

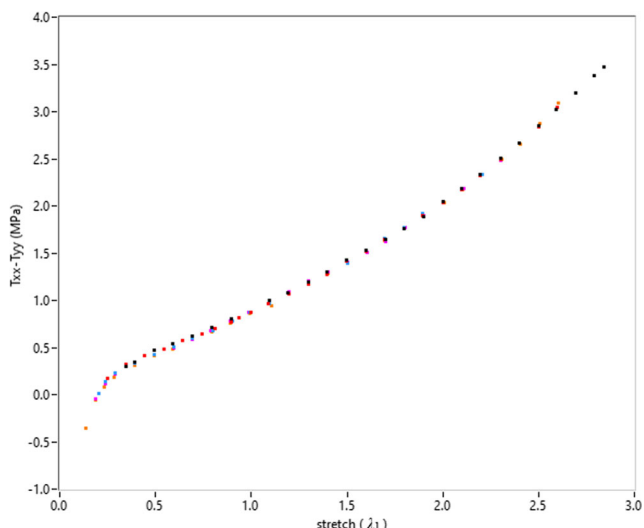


Fig. 7 Biaxial data from Fig. 6 are shifted up to a single curve using Eq. (15) with coefficients $m_1 = 0.890$ MPa and $m_2 = 0.0478$ MPa. These moduli fit data for $\lambda_1 > 0.5$ in Fig. 6 with correlation $R^2 = 0.9997$ and deviation RMSE = 0.0202 MPa, which is about 0.4% of full scale for 103 points

become fully extended. In this case, the parameter β increases with tensile strain for rubber-like materials described by the model (12).

Expressions for the nominal stress component P_{xx} predicted by (12) are obtained from results in Appendix 3 with m_2 replaced by $m_2/[1 - \beta(I_1 - 3)]$. As shown in Fig. 3, these expressions accurately fit Treloar’s loading data to $|\mathbf{V}| = 5$ with R^2 similar to the value in Fig. 1. The parameter β decreases by 62% ($0.045 \rightarrow 0.017$) as the limiting magnitude goes from 5 to 3.5, becoming negative for $|\mathbf{V}| = 3.4$. This sign change suggests an upper bound on the hyperelastic range, where a similar fit is obtained out to $|\mathbf{V}| = 3.5$ using model (7) or (12). Strain-induced crystallization may dominate uniaxial response for $\lambda > 7$, leading to hardening shown in Fig. 3. The constitutive Eq. (12) underestimates this response at large tensile strains similar to Ogden’s model (1972a, Fig. 4). This deviation suggests a hardening mechanism is active at very large strains.

The constitutive Eq. (12) is not derivable from an energy function, which allows *work in closed processes* (Gurtin 1981 p. 185). Such materials can unload along a different path, where the area between curves is the work per volume associated with a cycle. Hyperelastic solids must traverse the loading curve during this cycle, resulting in no hysteresis. However, at least part of the stress (12) is derivable from an energy function, since the alternate form

$$\mathbf{T} = -p\mathbf{I} + m_1\mathbf{V} + m_2I_2\mathbf{V}^2/3 + m_2\beta(I_1-3)I_2\mathbf{V}^2/3[1-\beta(I_1-3)], \tag{13}$$

splits this constitutive equation into model (7) and a term involving β that can dissipate energy (see Appendix 2). This term

is about 9.2% of total stress for planar and 19% for uniaxial and equibiaxial extension at the limit of fitted data in Fig. 3. This additive decomposition is consistent with observations by Göritz (1992) on filled and unfilled rubber. This electron microscopy study suggests that highly oriented short chains can significantly influence stress for these materials. These chains limit extensibility leading to hysteresis at intermediate to large strains associated here with positive values of β .

Hardening of vulcanized natural rubber at large strain is associated with chains aligning in the direction of extension (Treloar 2009 p. 20–23). The constitutive Eq. (12) can be modified to predict effects of strain-induced crystallization by adding a hardening term. For example, the equation

$$\mathbf{T} = -p\mathbf{I} + m_1\mathbf{V} + m_2I_2\mathbf{V}^2/3\left\{1-\beta\left[(I_1-3) + \alpha(I_2-3)^3\right]\right\} \tag{14}$$

adds a term associated with the dimensionless parameter α to fit Treloar’s extensional data shown in Fig. 4. This model can be split like (12)

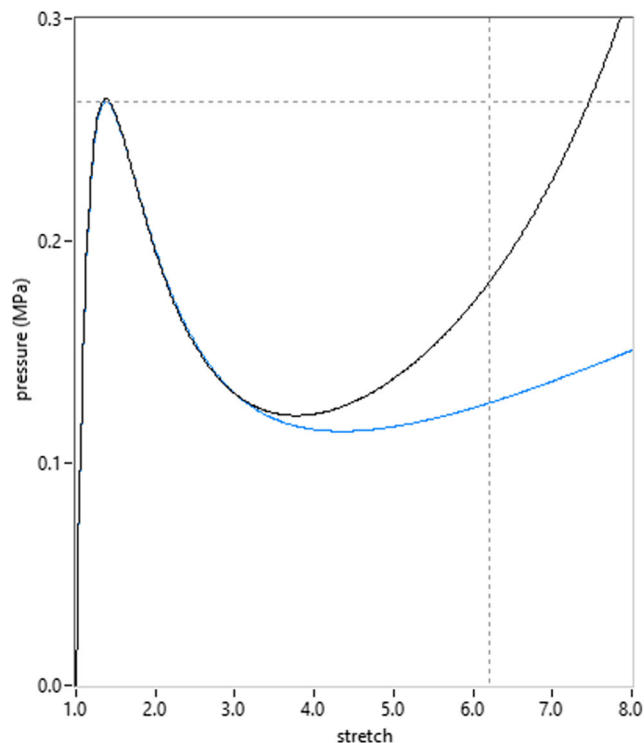


Fig. 8 A plot of scaled pressure P as a function of tangential stretch λ for a spherical balloon using both forms of Eq. (16). The lower curve uses moduli $m_1 = 0.740$ MPa and $m_2 = 0.0261$ MPa from Fig. 1, while the upper curve uses parameters $m_1 = 0.762$ MPa, $m_2 = 0.0216$ MPa, and $\beta = 0.0446$ from Fig. 3. Both curves have a maximum $P = 0.263$ MPa at $\lambda = 1.375$ followed by a pressure minimum outside the hyperelastic range. The lower curve increases along a straight line after the minimum, while the upper curve becomes unbounded for $\lambda \approx 11.95$. This point decreases to $\lambda \approx 6.2$ using results for the model (14) with parameters from Fig. 4. This limit suggests a bound on the size at rupture as shown in the figure

$$\mathbf{T} = -p\mathbf{I} + m_1\mathbf{V} + m_2I_2\mathbf{V}^2/3 + m_2\beta \left[(I_1-3) + \alpha(I_2-3)^3 \right] I_2\mathbf{V}^2/3 \left\{ 1 - \beta \left[(I_1-3) + \alpha(I_2-3)^3 \right] \right\}$$

into the constitutive Eq. (7) and a term involving α and β that can dissipate energy. Like (13), this term is not derivable from an energy function for m_1 constant. The parameter α decreases by 94% ($4.04\text{E-}5 \rightarrow 0.248\text{E-}5$) as the limiting magnitude goes from 5.4 to 4.5. A similar fit is obtained out to $|\mathbf{V}| = 5$ using model (12) or (14), which suggests a lower bound on the stretch magnitude associated with hardening. However, the additional term in (14) may only be necessary for filled rubber (see Appendix 5) or natural rubber at sufficiently large strains. For example, model (12), corresponding to $\alpha = 0$, is sufficient to describe extensional and shear data shown in Appendix 5 for a variety of rubber-like materials.

Treloar’s uniaxial data shown in Fig. 5 displays extensive hysteresis during unloading, which is not predicted by constitutive equations for hyperelastic materials. The unloading curve requires a modified version of (14), where the hardening term exponent is increased from 3 to 5. This modified model accurately fits both loading and unloading curves shown in the figure, but does not do as well with data in Fig. 4. The work per volume associated with this closed cycle is the area 2.24 MPa between these curves. The shear modulus $\mu = m_1/2 + m_2$ drops 16% ($0.415 \rightarrow 0.347$ MPa) for the unloading curve. Parameters β and α decrease from positive values during tensile loading to negative values for the unloading curve. The drop in β is consistent with a dynamic constraint $\beta I_2 \geq 0$ imposed by dissipation (see Appendix 2), where the invariant I_2 decreases during the unloading phase. Plotting this invariant as a function of λ yields a convex curve with a minimum at $\lambda = 1$. Consequently, the parameter β should also be negative while unloading from compressive stresses outside the hyperelastic range. The dynamic constraint further suggests that dissipative stress associated with β can play a significant role in shear wave propagation and other unsteady motions.

While agreement with Treloar’s extensional data is encouraging, the parameter β associated with limited extensibility exhibits a complicated dependence on invariants of \mathbf{V} . Assume β is an increasing function of $J - 1$, where the isochoric constraint $J = \det(\mathbf{V}) = 1$ becomes a *less accurate approximation* outside the hyperelastic range. Since volume increases for rubber subject to tensile stress (Penn 1970), the density ρ should decrease relative to the reference state value ρ_0 . In this case, the expression $J = \rho_0/\rho$ (Gurtin 1981 p. 88) implies a positive value for β that *increases* with tensile stress. The 13% drop in β between Figs. 3 and 4 is consistent with *volume reduction* during strain-induced crystallization (Treloar 2009 pp. 22–23). A similar argument suggests that β becomes *negative and decreases* with compressive stress. This parameter could also depend on the material rate \dot{J} as well as I_2 to exhibit the decrease during unloading shown in

Fig. 5. Pressure should be specified as a function of invariants (Ogden 1972b) to model materials as compressible.

The special case (12) obtained by setting $\alpha = 0$ in the constitutive Eq. (14) is sufficient to fit Jones and Treloar’s biaxial data (see Ogden 1984 p. 494). The normal stress difference $N_1 = T_{xx} - T_{yy}$ obtained from Appendix 3 is plotted as a function of stretches λ_1 and λ_2 in Fig. 6. As expected, the parameter β is negative for compressive stresses, increasing from -0.36 to -0.0092 as the minimum λ_1 stretch goes from 0.18 to 0.5. For $\lambda_1 > 0.5$, the special case (7) accurately fits biaxial data ($R^2 = 0.9997$) in Fig. 6 since $\beta \approx 0$. If additional data were available at larger strains, a separate fit with positive β might be required to describe tensile stress outside the hyperelastic range. Note that non-zero values of β imply hysteresis for a similar vulcanized natural rubber tested by Treloar (1944). Also note that uniaxial and equibiaxial extension bound biaxial response in the I_1 – I_2 plane similar to descriptions by Urayama (2006) and Treloar (2009 p. 218) using invariants $\text{tr}(\mathbf{B})$ and $\text{tr}(\mathbf{B}^{-1})$.

The exceptional fit of biaxial data in Fig. 6 is aided by separability of the associated energy function (9). The normal stress difference in biaxial extension predicted by model (7) has the alternate form

$$N_1 = \lambda_1 \widehat{W}(\lambda_1) - \lambda_2 \widehat{W}(\lambda_2), \quad \widehat{W}(\lambda) = m_1 + m_2(\lambda^3 - \lambda^{-3})/3 \quad (15)$$

implying a vertical shift $\lambda_2 \widehat{W}(\lambda_2)$ between curves in the hyperelastic range. Extending this result by replacing m_2 with $m_2/[1 - \beta(I_1 - 3)]$ essentially skews the shift between curves. However, Treloar (2009 p. 243) successfully superposed all data in Fig. 6 to a single curve. A similar result is obtained in Fig. 7 by applying the shift factor $\lambda_2 \widehat{W}(\lambda_2)$ in Eq. (15), where constants m_1 and m_2 fit biaxial data for $\lambda_1 > 0.5$. This simple shift does surprisingly well at aligning points outside the hyperelastic range ($\lambda_1 < 0.5$). This result highlights the extended role separability plays in describing biaxial data in Fig. 6.

Equibiaxial tension approximates the state of stress in a spherical balloon, where tangential stress components $T_{\phi\phi} \approx T_{\theta\theta}$ are nearly equal. The volume of material is about $4\pi t_0 R_0^2$ for a thin-walled balloon ($t_0/R_0 < 0.1$) with initial radius R_0 and thickness t_0 . An inflated balloon with radius R and thickness t has the approximate volume $4\pi t R^2$. Deformation is isochoric if $t/t_0 \approx (R/R_0)^{-2}$, where the *tangential stretch* $\lambda = R/R_0$ is essentially a ratio of arc lengths. A force balance on a hemispherical section implies $2\pi t R T_{\phi\phi} \approx \pi R^2 p_g$ in terms of the *gage pressure* p_g . Applying the isochoric constraint leads to an approximation $P \approx T_{\phi\phi}/\lambda^3$ for the *scaled pressure* $P = p_g R_0/2 t_0$. This approximation becomes a function of tangential stretch

$$P \approx m_1(\lambda^2 - \lambda^{-5}) + m_2(\lambda^{-1} - \lambda^{-7})(2\lambda^2 + \lambda^{-4})/3 \quad (16)$$

using the equibiaxial result for T_{xx} in Appendix 3. Replacing m_2 with $m_2/[1 - \beta(2\lambda + \lambda^{-2} - 3)]$ extends (16) beyond the hyperelastic range. The resulting expression exhibits limited extensibility, where P becomes unbounded at λ corresponding to the largest positive root of the polynomial $2\lambda^3 - (3 + \beta^{-1})\lambda^2 + 1 = 0$. Both expressions for scaled pressure are plotted in Fig. 8 using material parameters for vulcanized natural rubber.

Curves in Fig. 8 exhibit a pressure maximum at small strains first observed by Osborne (1909) for rubber balloons. This point is measurable in experiments that control the volume of air in a balloon. Varga's model (1966 p. 154) predicts a pressure maximum at $\lambda = (5/2)^{1/3} \approx 1.357$, while Ogden (1972a) calculated the value $\lambda = [(2\alpha_1 + 3)/(3 - \alpha_1)]^{1/3\alpha_1}$ for $-3/2 < \alpha_1 < 3$ using the first term in (4). If $m_2 > 0$ and $0 < m_2/m_1 < 0.18768$, the maximum predicted by (16) occurs in the range $1.357 < \lambda < 1.888$ followed by a pressure minimum shown in Fig. 8. For comparison, the Mooney–Rivlin model (2) exhibits a maximum in the range $1.383 < \lambda < 1.840$ if $C_2 > 0$ and $0 < C_2/C_1 < 0.21446$ (Mangan and Destradre 2015). The scaled pressure (16) is a strictly increasing function of λ if $m_2 > 0$ and $m_2/m_1 > 0.18768$. The constraint $m_2/m_1 < -0.5$ implies a positive shear modulus $\mu = m_1/2 + m_2$ for $m_1 < 0$ and $m_2 > 0$. In this case, the pressure (16) is also a strictly increasing function of λ like the predicted curve for porcine liver tissue in Appendix 5.

Discussion

The model (14) based on the left stretch tensor \mathbf{V} describes rubber-like materials using four parameters linked to physical processes observed in specific ranges of deformation. This constitutive equation describes hysteresis at intermediate to large strains as a consequence of limited extensibility, while the effect of crystallization at very large strains is modeled using a simple hardening term. The parameter α associated with this term vanishes at smaller tensile strains, reducing (14) to the model (12). The parameter β associated with limited extensibility tends to decrease in compression and increase in tension, with a slight decrease at very large tensile strains. This behavior suggests a dependence on density as the isochoric constraint becomes less accurate at larger strains. An abrupt drop to negative values during uniaxial unloading is consistent with a dynamic constraint imposed by dissipation. The parameter β vanishes for intermediate to small strains, reducing (12) and (14) to the constitutive Eq. (7). This equation describes hyperelastic solids, where remaining parameters satisfy the constraint $m_1/2 + m_2 > 0$ ensuring a positive shear modulus. This model can be derived from an energy function (9), which is convex if $m_2 \geq 0$. This function can be expressed in the separable form (10), which is a special case of Ogden's model (4). The modulus m_1 determines a Poynting effect predicted by Eqs. (7), (12), and (14) for rubber-like materials.

Data correlation for a wide variety of materials, including natural and synthetic rubber as well as soft tissue, suggest the utility of simple constitutive equations based on the left stretch tensor \mathbf{V} . Specifically, the model (14) and special cases (12) and (7) provide excellent results with $R^2 > 0.995$ over a large range of deformation for biaxial, planar, and uniaxial extension. The Varga term involving m_1 is essential to this capability as well as predictions in simple shear and the inflation of spherical membranes. An equivalent expression in terms of the left Cauchy–Green tensor \mathbf{B} is significantly more complicated, requiring the positive root of a quartic equation. While guessing this expression seems unlikely, simpler models based on \mathbf{B} have failed to describe the *entire range of behavior* shown here. Regarding the proposed description of hysteresis, Ericksen's (1977) prescient advice seems appropriate.

“Gradually, it has become clear that elasticity theory can predict effects that we do not commonly think of as being associated with the adjective elastic. In such

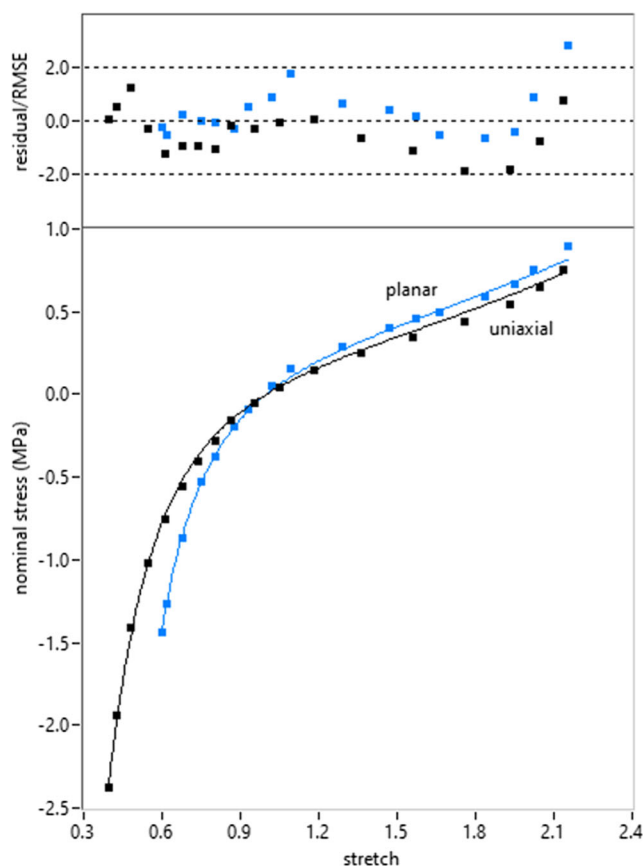


Fig. 9 A fit of planar and uniaxial data (Meunier et al. 2008) for unfilled silicone rubber using Eq. (12), where coefficients $m_1 = 0.262$ MPa, $m_2 = 0.190$ MPa, and $\beta = -0.404$ determine curves with correlation $R^2 = 0.9989$, relative error $E = 10.4\%$, and $SSE = 0.024$ (MPa) 2 . Distribution of error is normalized by $RMSE = 0.0275$ MPa, which is about 0.8% of full scale for 35 data points shown in the figure

cases, we should, I think, let elasticity theory enter into free competition with other theories capable of describing the effect at hand.”

Regardless of the outcome, constitutive equations presented here provide a useful starting point for accurately describing rubber-like materials in terms of an objective measure of deformation.

Acknowledgments The application [WebPlotDigitizer 4.1](#) was used to obtain numerical data from plot images. This exceptional program is copyrighted by the developer Ankit Rohatgi. Plot images were obtained directly from PDF files using [Snagit 2019](#) or scanned from books (Figs. 5 and 6) using an Epson Perfection V700 Photo flatbed scanner. All graphs were generated using software developed in LabVIEW 2018. This software is available upon request as a LabVIEW project or a compiled Windows application requiring the LabVIEW 2018 32-bit Runtime.

Appendices

Model conversion

For isochoric deformation, the left stretch tensor \mathbf{V} satisfies the Cayley–Hamilton equation (Gurtin 1981 p. 16)

$$\begin{aligned} \mathbf{V}^3 - \iota_1 \mathbf{V}^2 + \iota_2 \mathbf{V} &= \mathbf{I}, \iota_1 = \text{tr}(\mathbf{V}) = I_1, \iota_2 \\ &= [\text{tr}(\mathbf{V})^2 - \text{tr}(\mathbf{V}^2)]/2 = (I_1^2 - I_2)/2, \end{aligned}$$

where the principal invariants (ι_1, ι_2) are expressed in terms of the moment invariants (I_1, I_2) . Multiplying this equation by \mathbf{V}^{-2} and taking the trace implies the second result

$$\text{tr}(\mathbf{B}) = \text{tr}(\mathbf{V}^2) = I_2, \text{tr}(\mathbf{B}^{-1}) = \text{tr}(\mathbf{V}^{-2}) = (I_1^2 - I_2)^2 / 4 - 2I_1$$

relating $\text{tr}(\mathbf{B}^{-1})$ to moment invariants of \mathbf{V} , where $\mathbf{B} = \mathbf{V}^2$. These results are used to convert function (1) into an expression

$$\begin{aligned} w &= C_1 [\text{tr}(\mathbf{B}) - 3] + C_2 [\text{tr}(\mathbf{B}^{-1}) - 3] \\ &= C_1 (I_2 - 3) + C_2 \left[(I_1^2 - I_2)^2 / 4 - 2I_1 - 3 \right] \end{aligned}$$

involving stretch tensor invariants, where C_1 and C_2 are constants. Using this energy function in (8) leads to an alternate form of the constitutive Eq. (2)

$$\mathbf{T} + p\mathbf{I} = C_2 (I_1^3 - I_1 I_2 - 2) \mathbf{V} + [2C_1 + C_2 (I_2 - I_1^2)] \mathbf{V}^2,$$

where the shear modulus $\mu = 2(C_1 + C_2)$ is positive. See Treloar (2009 pp. 211–229) for further discussion of the Mooney–Rivlin model.

The left stretch tensor can be expressed in terms of \mathbf{B} using the Cayley–Hamilton equation for \mathbf{V} . Multiplying this equation by \mathbf{V} gives an alternate form

$$\mathbf{V}^4 - \iota_1 \mathbf{V}^3 + \iota_2 \mathbf{V}^2 = \mathbf{V}$$

in terms of principal invariants (ι_1, ι_2) . Substituting for \mathbf{V}^3 using the Cayley–Hamilton equation results in the expression

$$\mathbf{B}^2 + (\iota_2 - \iota_1^2) \mathbf{B} - \iota_1 \mathbf{I} = (1 - \iota_1 \iota_2) \mathbf{V},$$

where $\mathbf{B} = \mathbf{V}^2$. Solving for \mathbf{V} leads to an expression

$$\mathbf{V} = [\mathbf{B}^2 - (I_2 + I_1^2) \mathbf{B} / 2 - I_1 \mathbf{I}] / [1 - I_1 (I_1^2 - I_2) / 2],$$

involving moment invariants $I_1 = \text{tr}(\mathbf{V})$ and $I_2 = \text{tr}(\mathbf{V}^2) = \text{tr}(\mathbf{B})$. This expression can be written in terms of \mathbf{B}^{-1} and \mathbf{B} using a result

$$\mathbf{B}^2 = \mathbf{B}^{-1} + \text{tr}(\mathbf{B}) \mathbf{B} - \text{tr}(\mathbf{B}^{-1}) \mathbf{I}$$

obtained from the Cayley–Hamilton equation for \mathbf{B} . A real root of the quartic equation

$$[I_1^2 - \text{tr}(\mathbf{B})]^2 / 4 - 2I_1 = \text{tr}(\mathbf{B}^{-1})$$

determines $I_1 \geq 3$ as a function of invariants $\text{tr}(\mathbf{B})$ and $\text{tr}(\mathbf{B}^{-1})$. Ogden (1972a) alluded to the complexity of this isotropic function in the context of Varga’s (1966) model. See Hoger and Carlson (1984), Ting (1985), and Sawyers (1986) for a generalization where $\det(\mathbf{V}) \neq 1$.

Constitutive equations for elastic solids determine Cauchy stress $\mathbf{T} = \mathbf{S}(\mathbf{F})$ as a function of the deformation gradient \mathbf{F} . This function satisfies the constraint $\mathbf{S}(\mathbf{F}) = \mathbf{S}(\mathbf{F}\mathbf{H})$, where the symmetry transformation \mathbf{H} is a constant rotation for isotropic materials. The polar decomposition $\mathbf{F} = \mathbf{V}\mathbf{R}$ leads to a necessary condition $\mathbf{S}(\mathbf{F}) = \mathbf{S}(\mathbf{V}\mathbf{R}\mathbf{H}) = \mathbf{S}(\mathbf{V})$ associated with the material rotation $\mathbf{R} = \mathbf{H}^T$. The constitutive function also satisfies the constraint $\mathbf{S}(\mathbf{Q}\mathbf{V}\mathbf{Q}^T) = \mathbf{Q}\mathbf{S}(\mathbf{V})\mathbf{Q}^T$, where $\mathbf{Q}(t)$ is a time-dependent rotation associated with a change of frame. This constraint implies the general model (6) for incompressible elastic solids. Substituting a complicated expression for \mathbf{V} in terms of \mathbf{B} , which is implicit in Gurtin’s derivation (1981 p. 167), leads to an alternate form of the general model. This result suggests that basic constitutive equations involving the natural variable \mathbf{V} might provide a better description of isotropic elastic solids than simple models using the substitute variable \mathbf{B} .

Hyperelastic solids

An incompressible elastic solid described by the constitutive eq. $\mathbf{T} = -p\mathbf{I} + \mathbf{S}(\mathbf{V})$ is hyperelastic if the symmetric tensor $\mathbf{S}(\mathbf{V})$ can be derived from a scalar energy function of the left

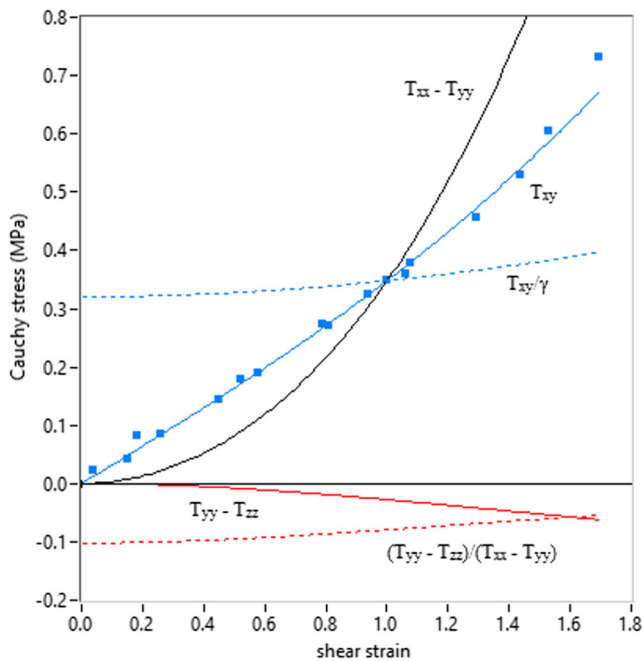


Fig. 10 Shear stress values derived from planar extension data for an unfilled silicone rubber in Fig. 9 using the equivalence relations (11). An absolute value is used to map all data to this quadrant. Curves are predictions of Eq. (12) using coefficients from Fig. 9 with correlation $R^2 = 0.9907$ to derived data. Deviation from predicted values is $RMSE = 0.0209$ MPa or about 1.8% of full scale over the entire range of shear strain ($-1.07 \rightarrow 1.62$). The ratio T_{xy}/γ increases from an initial value $\mu = m_1/2 + m_2 = 0.321$ MPa, while the ratio $(T_{yy} - T_{zz})/(T_{xx} - T_{yy})$ increases from $-m_1/8\mu = -0.102$ to zero. This material should exhibit *axial elongation* in torsion since $m_1 > 0$

stretch tensor \mathbf{V} . Assume the Cauchy stress \mathbf{T} satisfies an isothermal form of *Planck's inequality* (Truesdell 1984 pp. 112–115)

$$\mathbf{T} \cdot \mathbf{L} - \rho \dot{\psi} \geq 0$$

involving the *spatial velocity gradient* \mathbf{L} , *density* ρ , and a material derivative of the *specific free energy function* $\psi(\mathbf{V})$, where the *scalar product* $\mathbf{A} \cdot \mathbf{B} = \text{tr}(\mathbf{A}^T \mathbf{B})$ is defined for any tensors \mathbf{A} and \mathbf{B} in terms of the *trace function* (Gurtin 1981 p. 5). For incompressible solids, this constraint reduces to

$$\mathbf{S} \cdot \mathbf{L} - \dot{w} \geq 0,$$

where $w(\mathbf{V}) = \rho \psi$ is the *energy density function*. The chain rule implies

$$\dot{w} = \frac{\partial w}{\partial \mathbf{V}} \cdot \dot{\mathbf{V}},$$

which can be expressed as

$$\dot{w} = \frac{\partial w}{\partial \mathbf{V}} \mathbf{V} \cdot \mathbf{L}$$

using an identity (VanArsdale 2003)

$$\begin{aligned} \dot{\mathbf{V}} + \mathbf{V}\mathbf{W}_R - \mathbf{W}_R\mathbf{V} &= \mathbf{L}_D\mathbf{V}, \quad \mathbf{L} = \mathbf{W}_R + \mathbf{L}_D \\ &= \dot{\mathbf{R}}\mathbf{R}^T + \mathbf{R}\dot{\mathbf{U}}\mathbf{U}^{-1}\mathbf{R}^T \end{aligned}$$

associated with a polar decomposition $\mathbf{F} = \mathbf{R}\mathbf{U} = \mathbf{V}\mathbf{R}$ of the deformation gradient in terms of a material rotation \mathbf{R} and symmetric stretch tensors \mathbf{U} and \mathbf{V} with positive principle values. Since the stress \mathbf{S} and energy density w are independent of \mathbf{L} , the isothermal form of Planck's inequality is satisfied only if

$$\mathbf{S} = \frac{\partial w}{\partial \mathbf{V}} \mathbf{V},$$

where this material *does not dissipate energy* in any isochoric motion. Since w is an isotropic function of \mathbf{V} , the energy density can be expressed as $\hat{w}(I_1, I_2)$ in terms of the *moment invariants* $I_1 = \text{tr}(\mathbf{V})$ and $I_2 = \text{tr}(\mathbf{V}^2)$ (Gurtin 1981 p. 230). The resulting partial derivative

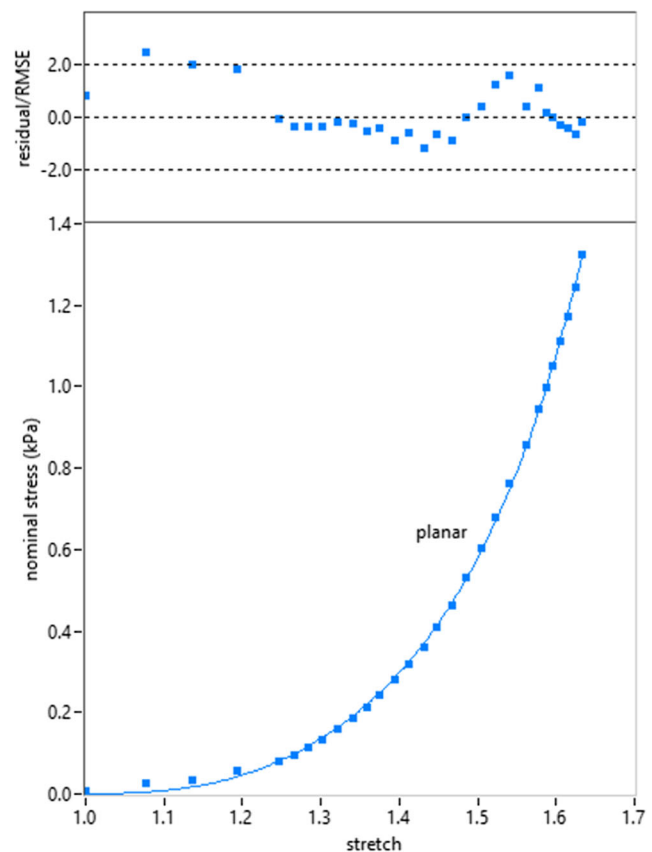


Fig. 11 A fit of planar extension data (Gao et al. 2010) for porcine liver tissue using Eq. (12), where coefficients $m_1 = -0.946$ kPa, $m_2 = 0.479$ kPa, and $\beta = 2.14$ determine curves with correlation $R^2 = 0.9996$, relative error $E = 4.4\%$, and $SSE = 0.0012$ (kPa)². Distribution of error is normalized by $RMSE = 0.00866$ kPa, which is about 0.7% of full scale for 29 data points shown in the figure. Note that the shear modulus $\mu = m_1/2 + m_2 = 0.006$ kPa is positive for this soft tissue

$$\frac{\partial w}{\partial \mathbf{V}} = \frac{\partial \hat{w}}{\partial I_1} \mathbf{I} + 2 \frac{\partial \hat{w}}{\partial I_2} \mathbf{V}$$

leads to the expression (8) for stress in terms of the moment invariants.

However, only some models described by the general constitutive Eq. (6) have this property. For example, model (12) cannot be derived from an energy function but can be expressed in the alternate form (13). The preceding derivation suggests that one part is determined by an energy function, while the remaining stress can dissipate energy. The dissipation rate associated with this part

$$\frac{m_2 \beta (I_1 - 3) I_2 \mathbf{V}^2 \cdot \mathbf{L}}{3[1 - \beta(I_1 - 3)]} = \frac{m_2 \beta (I_1 - 3) I_2 \mathbf{V}^2 \cdot \dot{\mathbf{V}} \mathbf{V}^{-1}}{3[1 - \beta(I_1 - 3)]} = \frac{m_2 \beta (I_1 - 3) I_2 \dot{I}_2}{6[1 - \beta(I_1 - 3)]} \geq 0$$

is non-negative for $m_2 > 0$ if $\beta \dot{I}_2 \geq 0$ in dynamic processes. This constraint, which also applies to the constitutive Eq. (14), is consistent with the drop in β during uniaxial unloading from a large tensile strain shown in Fig. 5.

Model predictions

Predictions of model (7) with material constants m_1 and m_2 are listed below, where T_{xx} , T_{xy} , T_{yy} , T_{zz} , and P_{xx} denote Cauchy and nominal stress components associated with the orthonormal basis vectors $\vec{e}_x, \vec{e}_y, \vec{e}_z$. Deformation is characterized by the left stretch tensor \mathbf{V} and the deformation gradient \mathbf{F} , where symbols $\gamma, \lambda, \lambda_1, \lambda_2$ denote the shear strain and principal stretches in coordinate directions. Tensors are expressed as linear combinations of basis tensors defined using a tensor product (Gurtin 1981 p. 4). Predictions of the constitutive Eqs. (12) and (14) are obtained by replacing m_2 with $m_2/[1 - \beta(I_1 - 3)]$ or $m_2/\{1 - \beta[(I_1 - 3) + \alpha(I_2 - 3)^3]\}$ in the expressions below.

Uniaxial extension:

$$\begin{aligned} \mathbf{V} &= \lambda \vec{e}_x \otimes \vec{e}_x + \lambda^{-1/2} (\vec{e}_y \otimes \vec{e}_y + \vec{e}_z \otimes \vec{e}_z), \text{tr}(\mathbf{V}) \\ &= \lambda + 2\lambda^{-1/2}, \text{tr}(\mathbf{V}^2) = \lambda^2 + 2\lambda^{-1} \\ T_{yy} = T_{zz} = 0 \Rightarrow p &= m_1 \lambda^{-1/2} + m_2 \lambda^{-1} \text{tr}(\mathbf{V}^2)/3 \Rightarrow T_{xx} \\ &= m_1 (\lambda - \lambda^{-1/2}) + m_2 (\lambda^2 - \lambda^{-1}) \text{tr}(\mathbf{V}^2)/3 \\ \mathbf{F} &= \lambda \vec{e}_x \otimes \vec{e}_x + \lambda^{-1/2} (\vec{e}_y \otimes \vec{e}_y + \vec{e}_z \otimes \vec{e}_z) \Rightarrow P_{xx} \\ &= m_1 (1 - \lambda^{-3/2}) + m_2 (\lambda - \lambda^{-2}) (\lambda^2 + 2\lambda^{-1})/3 \end{aligned}$$

Planar extension:

$$\begin{aligned} \mathbf{V} &= \lambda \vec{e}_x \otimes \vec{e}_x + \vec{e}_y \otimes \vec{e}_y + \lambda^{-1} \vec{e}_z \otimes \vec{e}_z, \text{tr}(\mathbf{V}) \\ &= \lambda + 1 + \lambda^{-1}, \text{tr}(\mathbf{V}^2) = \lambda^2 + 1 + \lambda^{-2} \\ T_{zz} = 0 \Rightarrow p &= m_1 \lambda^{-1} + m_2 \lambda^{-2} \text{tr}(\mathbf{V}^2)/3 \Rightarrow T_{xx} \\ &= m_1 (\lambda - \lambda^{-1}) + m_2 (\lambda^2 - \lambda^{-2}) \text{tr}(\mathbf{V}^2)/3 \\ \mathbf{F} &= \lambda \vec{e}_x \otimes \vec{e}_x + \vec{e}_y \otimes \vec{e}_y + \lambda^{-1} \vec{e}_z \otimes \vec{e}_z \Rightarrow P_{xx} \\ &= m_1 (1 - \lambda^{-2}) + m_2 (\lambda - \lambda^{-3}) (\lambda^2 + 1 + \lambda^{-2})/3 \end{aligned}$$

Equibiaxial extension:

$$\begin{aligned} \mathbf{V} &= \lambda (\vec{e}_x \otimes \vec{e}_x + \vec{e}_y \otimes \vec{e}_y) + \lambda^{-2} \vec{e}_z \otimes \vec{e}_z, \text{tr}(\mathbf{V}) \\ &= 2\lambda + \lambda^{-2}, \text{tr}(\mathbf{V}^2) = 2\lambda^2 + \lambda^{-4} \\ T_{zz} = 0 \Rightarrow p &= m_1 \lambda^{-2} + m_2 \lambda^{-4} \text{tr}(\mathbf{V}^2)/3 \Rightarrow T_{xx} \\ &= m_1 (\lambda - \lambda^{-2}) + m_2 (\lambda^2 - \lambda^{-4}) \text{tr}(\mathbf{V}^2)/3 \\ \mathbf{F} &= \lambda (\vec{e}_x \otimes \vec{e}_x + \vec{e}_y \otimes \vec{e}_y) + \lambda^{-2} \vec{e}_z \otimes \vec{e}_z \Rightarrow P_{xx} \\ &= m_1 (1 - \lambda^{-3}) + m_2 (\lambda - \lambda^{-5}) (2\lambda^2 + \lambda^{-4})/3 \end{aligned}$$

Biaxial extension:

$$\begin{aligned} \mathbf{V} &= \lambda_1 \vec{e}_x \otimes \vec{e}_x + \lambda_2 \vec{e}_y \otimes \vec{e}_y + (\lambda_1 \lambda_2)^{-1} \vec{e}_z \otimes \vec{e}_z, \text{tr}(\mathbf{V}) \\ &= \lambda_1 + \lambda_2 + (\lambda_1 \lambda_2)^{-1}, \\ \text{tr}(\mathbf{V}^2) &= \lambda_1^2 + \lambda_2^2 + (\lambda_1 \lambda_2)^{-2}; T_{xx} - T_{yy} \\ &= m_1 (\lambda_1 - \lambda_2) + m_2 (\lambda_1^2 - \lambda_2^2) \text{tr}(\mathbf{V}^2)/3, \end{aligned}$$

Simple shear:

$$\begin{aligned} \mathbf{v} &= (4 + \gamma^2)^{-1/2} [(2 + \gamma^2) \vec{e}_x \otimes \vec{e}_x + \gamma (\vec{e}_x \otimes \vec{e}_y + \vec{e}_y \otimes \vec{e}_x) + 2 \vec{e}_y \otimes \vec{e}_y] \\ &\quad + \vec{e}_z \otimes \vec{e}_z, \\ \text{tr}(\mathbf{V}) &= 1 + (4 + \gamma^2)^{1/2}, \text{tr}(\mathbf{V}^2) = 3 + \gamma^2; T_{xy} \\ &= m_1 \gamma (4 + \gamma^2)^{-1/2} + m_2 \gamma (3 + \gamma^2)/3, \\ T_{xx} &= m_1 [(2 + \gamma^2)(4 + \gamma^2)^{-1/2} - 1] \\ &\quad + m_2 \gamma^2 (3 + \gamma^2)/3, T_{yy} \\ &= m_1 [2(4 + \gamma^2)^{-1/2} - 1], T_{zz} = 0 \end{aligned}$$

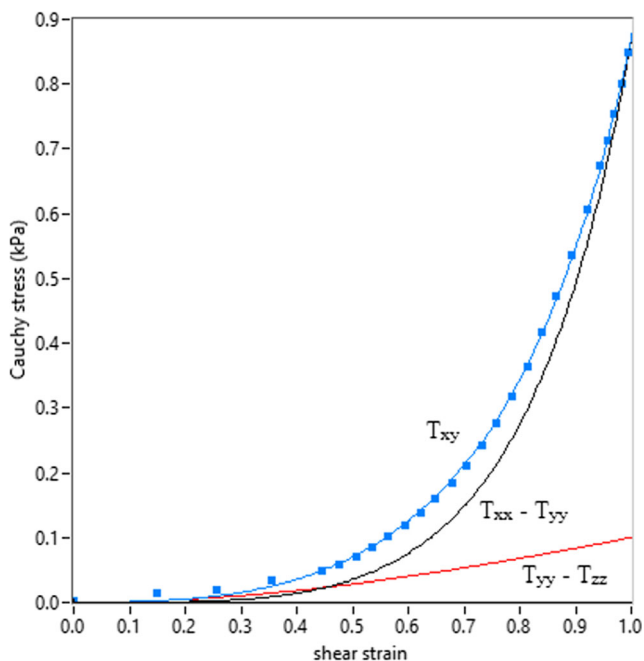


Fig. 12 Shear stress values derived from planar extension data for porcine liver tissue in Fig. 11 using the equivalence relations (11). Curves are predictions of Eq. (12) using coefficients from Fig. 11 with correlation $R^2 = 0.9997$ to derived data. Deviation from predicted values is $RMSE = 0.00545$ kPa or about 0.6% of full scale for data shown in the figure. Note that the secondary normal stress difference $T_{yy} - T_{zz}$ is positive. This material should exhibit *axial contraction* in torsion since $m_1 < 0$

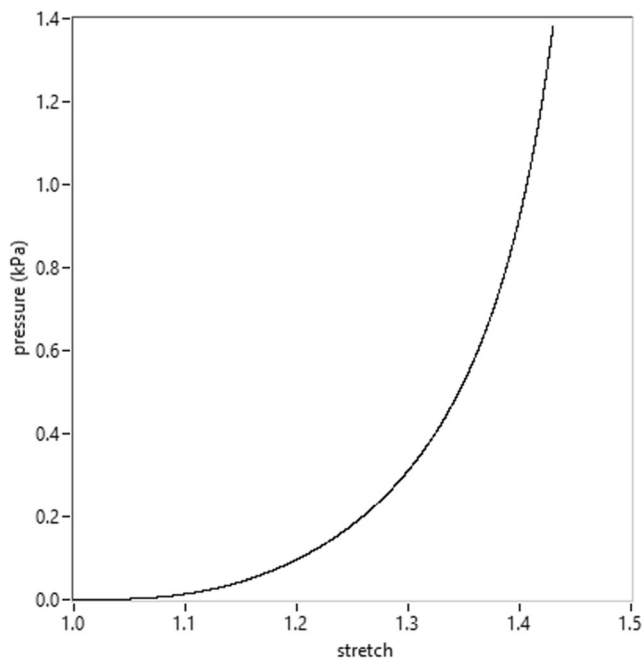


Fig. 13 Scaled pressure P as a function of tangential stretch λ for a spherical membrane using the extended version of Eq. (16) with coefficients from Fig. 11. This curve becomes unbounded for $\lambda > 1.516$, suggesting a limit on the size at rupture. This trend is qualitatively similar to measurements by Osborne (1909) on a monkey bladder as well as porcine sclera data obtained by Lari et al. (2012). These authors also observe hysteresis during sclera deflation and uniaxial unloading, which is consistent with $\beta \neq 0$

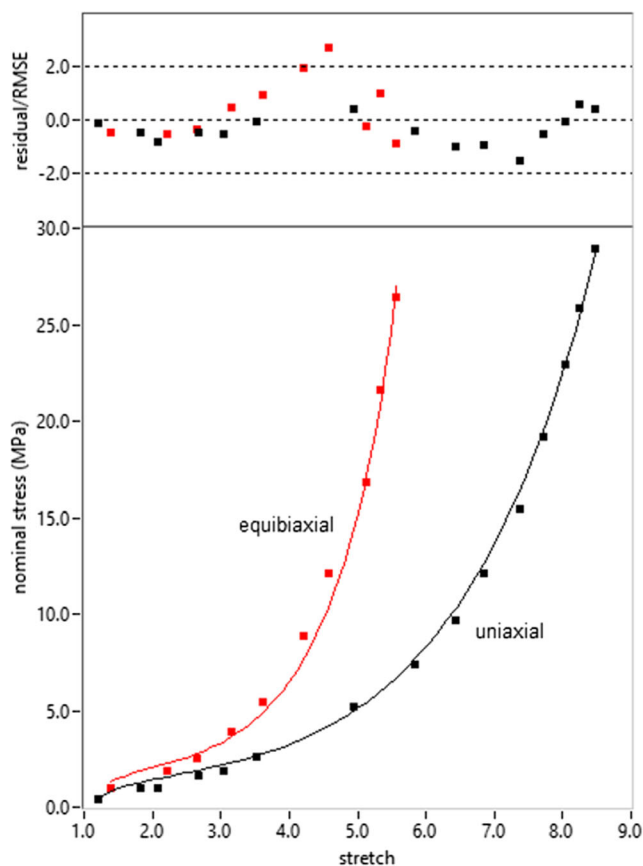


Fig. 14 A fit of equibiaxial and uniaxial data (Alexander 1968) for a synthetic rubber neoprene using Eq. (12), where coefficients $m_1 = 1.90$ MPa, $m_2 = 0.0597$ MPa, and $\beta = 0.0887$ determine curves with correlation $R^2 = 0.9958$, relative error $E = 54\%$, and $SSE = 8.7$ (MPa)². The distribution of error is normalized by $RMSE = 0.628$ MPa, which is about 2.2% of full scale for 25 data points shown in the figure

Fitting algorithm

The method used here searches for m model parameters that improve *goodness of fit* (also known as *coefficient of determination*)

$$R^2 = 1 - \frac{\sum_{i=0}^{n-1} (y_i - f_i)^2}{\sum_{i=0}^{n-1} (y_i - \bar{y})^2},$$

where predicted values f_i are compared to n measurements y_i with mean $\bar{y} = \sum y_i / n$. *Residuals* are errors $y_i - f_i$ associated with this correlation. The *root mean squared error*

$$RMSE = \sqrt{\frac{1}{n-m} \sum_{i=0}^{n-1} (y_i - f_i)^2}$$

is essentially the standard deviation of data about a fit with $n - m$ *degrees of freedom*. This statistic normalizes residuals plotted in most figures, suggesting a *confidence interval* for predicted values. Root mean squared error is compared with

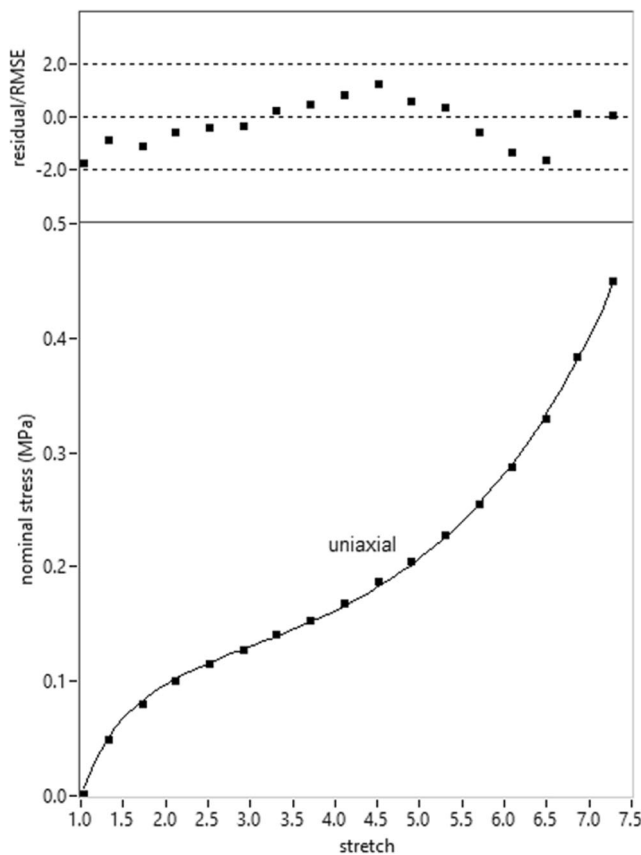


Fig. 15 A fit of uniaxial data (Fox and Goulbourne 2008) for polyacrylate rubber VHB 4905 using Eq. (12), where coefficients $m_1 = 0.144$ MPa, $m_2 = 0.00135$ MPa, and $\beta = 0.0872$ determine a curve with correlation $R^2 = 0.9994$, relative error $E = 1.1\%$, and $SSE = 0.00013$ (MPa)². The distribution of error is normalized by $RMSE = 0.00308$ MPa, which is about 0.7% of full scale for 17 data points shown in the figure. The value of β drops 79% to 0.0183 as the maximum stretch decreases to 6. A fit with $\beta = 0$ for $\lambda < 6$ has coefficients $m_1 = 0.137$ MPa and $m_2 = 0.00204$ MPa with correlation $R^2 = 0.9995$, which suggests an upper bound on the hyperelastic range for this material

the entire range of measurements $y_{max} - y_{min}$ to obtain *percent full scale*. *Relative errors* E_i are defined by Ogden et al. (2004) as absolute residuals $|y_i - f_i|$ normalized by the maximum of 0.5 or $|y_i|$. The *largest relative error* E and the *sum of squared error* $SSE = \sum (y_i - f_i)^2$ are provided with two significant digits for comparison with results in other papers. The goodness of fit is expressed with four significant digits, while model coefficients and the root mean squared error appear with three digits. A fit with $R^2 > 0.999$ and $RSME < 1\%$ full scale is considered excellent, while correlations with $R^2 < 0.99$ and $RSME > 2\%$ full scale are somewhat questionable for data shown in the figures.

The resulting algorithm randomly searches for new coefficients near the initial guess, where the change is usually less than 5% of the value. If a better fit is obtained with R^2 closer to one, the search resumes from the new set of coefficients. This process stops after a specified number of attempts (typically 1000) fails to improve the fit. Like most methods, this

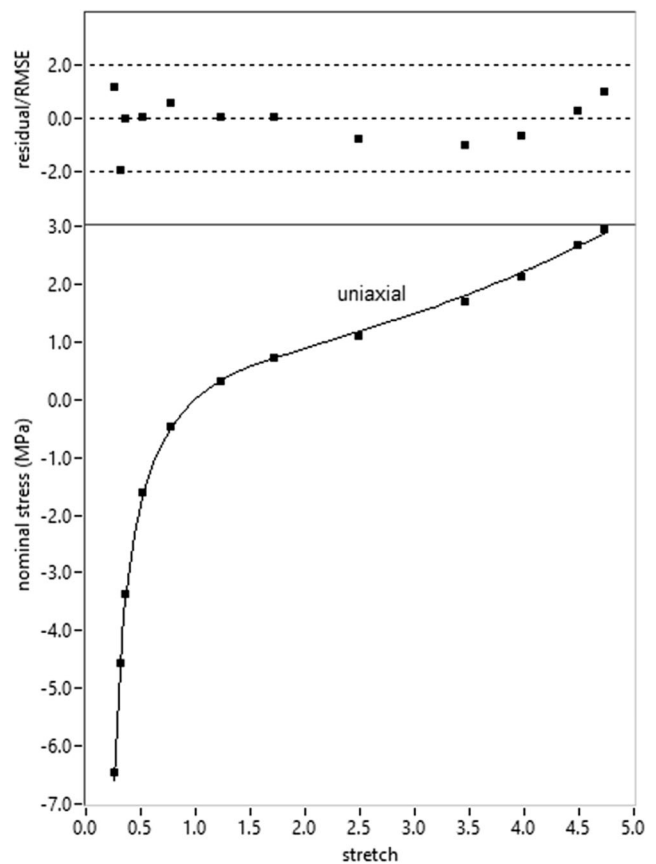


Fig. 16 A fit of uniaxial data (Yeoh and Fleming 1997) for a vulcanized rubber using Eq. (12), where coefficients $m_1 = 0.168$ MPa, $m_2 = 0.500$ MPa, and $\beta = -2.11$ determine a curve with correlation $R^2 = 0.9992$, relative error $E = 11.9\%$, and $SSE = 0.081$ (MPa)². The distribution of error is normalized by $RMSE = 0.0949$ MPa, which is about 1% of full scale for 12 data points shown in the figure

approach is sensitive to an initial guess. However, this guess can usually be refined in real time for $m < 4$ since the search only involves model evaluations. The resulting coefficients listed in figure captions concurrently fit all data displayed within the specified range except for Figs. 5 and 18. Shear stress predictions in Figs. 2, 10, and 12 do not involve this algorithm, where statistics are provided to characterize correlation with derived data.

An alternate approach is used by Ogden et al. (2004), where fitted values are determined using a least-squares analysis based on the function $SSE = \sum (f_i - y_i)^2$. These authors randomly vary their initial guess to improve this solution as determined by SSE and relative errors E_i . Plotting relative errors masks the trend of residuals (Curran-Everett 2011) by mapping all values to the positive quadrant. The significance of relative error is difficult to assess without additional information about experimental uncertainty. Since most test equipment has a fixed resolution, this uncertainty can be a large percentage of small data values. For example, Ogden et al. (2004) obtain relative errors up to 40% for small

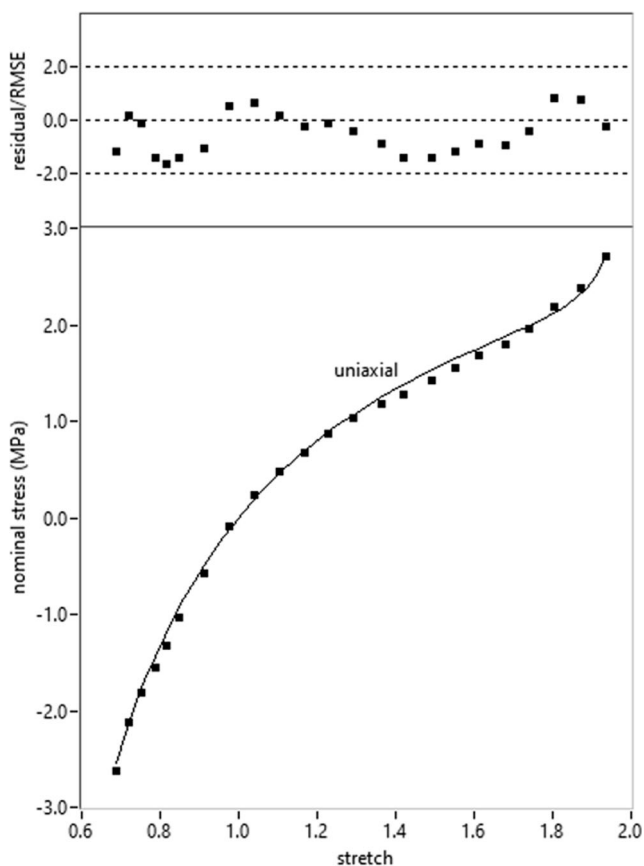


Fig. 17 A fit of uniaxial data (Miehe and Lulei 2001) for carbon black-filled rubber b186 using Eq. (12), where coefficients $m_1 = 3.28$ MPa, $m_2 = 0.0282$, and $\beta = 2.37$ determine a curve with correlation $R^2 = 0.9979$, relative error $E = 13.5\%$, and $SSE = 0.11$ (MPa)². The distribution of error is normalized by $RMSE = 0.0745$ MPa, which is about 1.4% of full scale for 23 data points shown in the figure. A better result can be obtained by fitting compressive and tensile stresses separately similar to Fig. 18

strains, where models seem to accurately describe extensional data. Smaller errors around 10% can occur at larger strains, where models visually deviate from data. Treloar's uniaxial and equibiaxial measurements are fit simultaneously by Ogden et al. (2004) to obtain a set of coefficients, while excluding planar extension data. This paper uses an energy function to describe Treloar's data well outside the hyperelastic range.

The approach in Ogden et al. (2004) is modified by Destrade et al. (2017), where fitted values are determined by minimizing the function $\Sigma[(f_i - y_i)/y_i]^2$ involving *relative residuals*. These authors must exclude measurements near zero to use this approach, which weights smaller values as more significant in determining a fit compared to a least-squares analysis by Ogden et al. (2004). This weighting is further exacerbated by an apparent choice of units, which stretches the y -axis by a factor of ten. At small strains, Destrade et al. (2017) obtain relative residuals around 15 to 20% for the *neo-Hookean* model even though fitted values appear

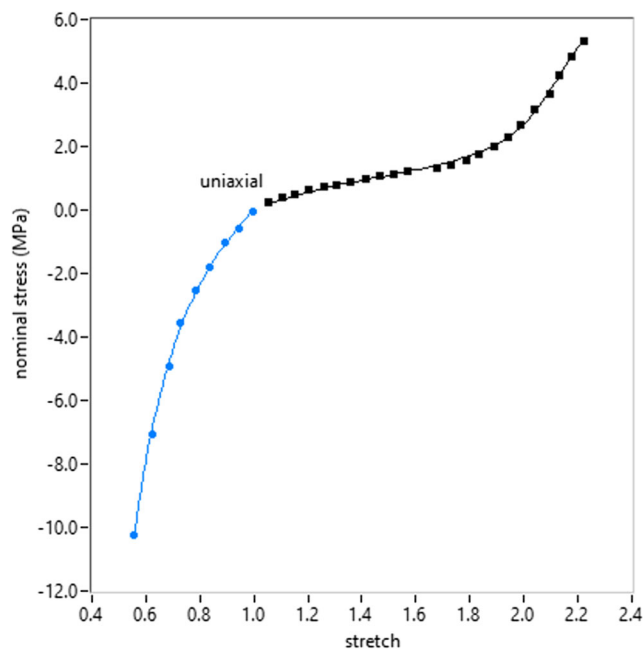


Fig. 18 Uniaxial data for carbon black-filled rubber NR 70 obtained by Bechir et al. (2006), where compressive (●) and tensile (■) stresses are fit separately using models (7) and (14). Coefficients $m_1 = -0.134$ MPa, $m_2 = 3.00$ MPa determine the compressive stress curve with shear modulus $\mu = 2.94$ MPa and correlation $R^2 = 0.9985$ $RMSE = 0.140$ MPa. Coefficients $m_1 = 2.04$ MPa, $m_2 = 0.0906$ MPa, $\beta = 2.27$, and $\alpha = -0.00713$ determine the tensile stress curve with shear modulus $\mu = 1.11$ MPa and correlation $R^2 = 0.9981$, $RMSE = 0.0681$ MPa

to accurately describe data deemed *most reliable*. They determine model coefficients by fitting just uniaxial data. See referee Martin Kroon's concern in [Supplemental Material](#) as well as observations by Urayama (2006) and Treloar (2009 p. 218) that uniaxial results are insufficient to distinguish between theories. Destrade et al. (2017, Fig. 9) limit predictions in simple shear to $\gamma \leq 1$ and do not compare with values derived from Treloar's planar extension data. They also use an energy function to describe Treloar's uniaxial data well outside the hyperelastic range ($\lambda < 5$). Neither this paper nor Ogden et al. (2004) provides guidance concerning the significance of any particular relative error.

Data comparisons

The constitutive Eq. (12) is used to fit extensional data obtained from Mansouri and Darijani (2014) for different rubber-like materials. Correlations in Figs. 9, 11, 14, 15, 16 and 17 have a goodness of fit $R^2 > 0.995$ and a root mean squared error $RMSE < 2.2\%$ of full scale. Predictions by (12) are similar to the best models evaluated by Mansouri and Darijani (2014, table 4) based on the sum of squared error SSE. In Figs. 10 and 12, simple shear predictions are compared with values

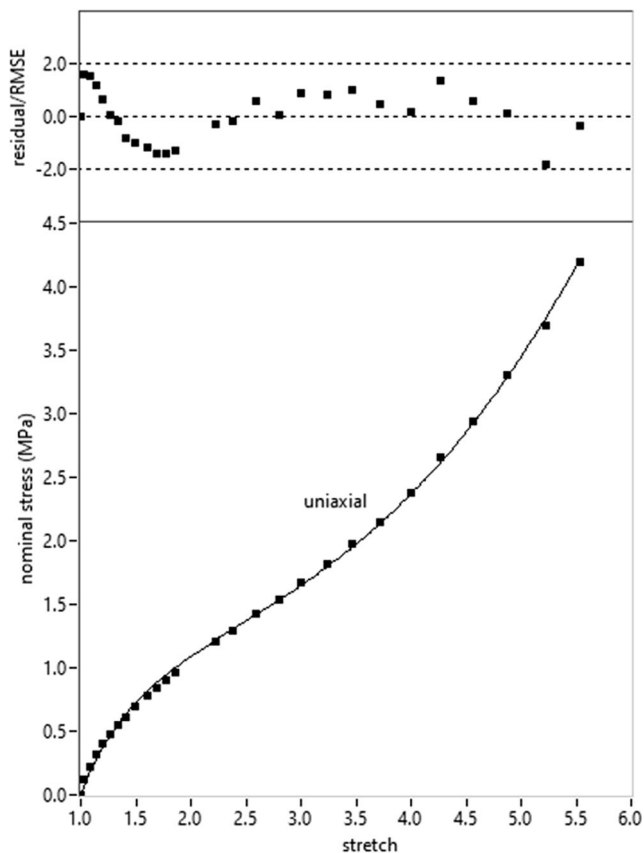


Fig. 19 A fit of uniaxial data (Dobrynin and Carrillo 2011) for rubber using Eq. (7), where coefficients $m_1 = 1.45$ MPa and $m_2 = 0.0506$ MPa determine a curve with correlation $R^2 = 0.9993$, relative error $E = 10.1\%$, and $SSE = 0.024$ (MPa) 2 . The distribution of error is normalized by $RMSE = 0.0311$ MPa, which is about 0.7% of full scale for 27 data points shown in the figure. This material should be hyperelastic over the entire range of deformation shown in the figure

derived from planar extension data using the equivalence relations (11). These predictions suggest axial elongation in torsion for silicone rubber, while the porcine liver tissue should exhibit a negative Poynting effect associated with axial contraction. A prediction for inflation of a spherical membrane is shown in Fig. 13 using parameters for porcine liver tissue. This plot is qualitatively similar to measurements on soft tissue by Osborne (1909) and Lari et al. (2012).

Uniaxial data shown in Fig. 18 are obtained from a plot in Bechir et al. (2006, Fig. 8b) for carbon black-filled vulcanized natural rubber. Separate curves for compressive and tensile stress are fit using models (7) and (14). Such an approach appears to be necessary for carbon black-filled rubber due to *amplification* (Yeoh 1990) at sufficiently large tensile strains, where *particle interactions* can lead to increased stiffness, tensile strength, and hysteresis (Omnès et al. 2008). While correlation is good, the predicted shear modulus $\mu = m_1/2 +$

m_2 is not continuous at $\lambda = 1$. An unusual negative value for α in (14) essentially keeps the tensile stress curve from becoming unbounded at large strains. While using six constants to fit uniaxial data seems excessive, Bechir et al. (2006, Fig. 9) obtain worse correlation, especially for compressive stress, with the same number of constants.

Values shown in Fig. 19 are obtained from a plot in Destrade et al. (2017, Fig. 2a), where stresses are about 9.8 times too large in the stated units N/mm^2 (Sec. 3a). These authors exclude the first 14 data points ($\lambda < 1.1$) from their analysis due to a *Mooney plot discrepancy* that they attribute to possible issues with the experiment. While some points are excluded here for $\lambda < 1.5$ due to large, overlapping plot symbols, scanned data do not exhibit the downturn shown in Destrade et al. (2017, Fig. 2c). This material is accurately described by model (7), which suggests hyperelastic behavior over the entire range of deformation shown in Fig. 19. The shear modulus $\mu = m_1/2 + m_2 = 0.777$ MPa predicted for this material is within $\pm 2\%$ of values ($0.761 \rightarrow 0.791$ MPa) obtained by Destrade et al. (2017, tables 2, 3, 5) using 12 different models for hyperelastic solids. However, these authors obtain a 14% variation in μ ($0.430 \rightarrow 0.492$ MPa) by fitting the same models to Treloar's (1944) uniaxial data (Destrade et al. 2017, tables 2, 3, 4), where some correlations involve data *outside the hyperelastic range*. These values are typically larger with greater variation than the shear modulus ($0.396 \rightarrow 0.431$ MPa) obtained for Treloar's (1944) loading data shown in Figs. 1, 3, 4, and 5.

References

- Alexander H (1968) A constitutive relation for rubber-like materials. *Int J Eng Sci* 6(9):549–563
- Arruda EM, Boyce MC (1993) A three-dimensional constitutive model for the large stretch behavior of rubber elastic materials. *J Mech Phys Solids* 41(2):389–412
- Bechir H, Chevalier L, Chaouche M, Boufala K (2006) Hyperelastic constitutive model for rubber-like materials based on the first Seth strain measures invariant. *Eur J Mech A Solids* 25(1):110–124
- Curran-Everett D (2011) Explorations in statistics: regression. *Adv Physiol Educ* 35:347–352
- Destrade M, Saccomandi G, Sgura I (2017) Methodical fitting for mathematical models of rubber-like materials. *Proc R Soc A* 473: 20160811
- Dobrynin AV, Carrillo J-MY (2011) Universality in nonlinear elasticity of biological and polymeric networks and gels. *Macromolecules* 44: 140–146
- Ericksen JL (1977) Special topics in elastostatics. *Adv Appl Mech* 17: 189–244
- Fox JW, Goulbourne NC (2008) On the dynamic electromechanical loading of dielectric elastomer membranes. *J Mech Phys Solids* 56(8): 2669–2686
- Gao Z, Lister K, Desai JP (2010) Constitutive modeling of liver tissue: experiment and theory. *Ann Biomed Eng* 38(2):505–516

- Gent AN (1996) A new constitutive relation for rubber. *Rubber Chem Technol* 69:59–61
- Görzt D (1992) Properties of rubber elastic systems at large strains. *Angew Makromol Chem* 202:309–329
- Gurtin ME (1981) *An introduction to continuum mechanics*. Academic Press, New York
- Hoger A, Carlson DE (1984) Determination of the stretch and rotation in the polar decomposition of the deformation gradient. *Q J Appl Math* 42:113–117 [PDF](#)
- Horgan CO, Ogden RW, Saccomandi S (2004) A theory of stress softening of elastomers based on finite chain extensibility. *Proc R Soc Lond A* 460:1737–1754
- Horgan CO, Smayda MG (2012) The importance of the second strain invariant in the constitutive modeling of elastomers and soft biomaterials. *Mech Mater* 51:43–52
- Hoss L, Marczak RJ (2010) A new constitutive model for rubber-like materials. *Mecánica Computacional XXIX*:2759–2773 [PDF](#)
- Hua CC, Schieber JD, Venerus DC (1999) Segment connectivity, chain-length breathing, segmental stretch, and constraint release in reptation models. III. Shear flows. *Soc Rheol* 43(3):701–717 [PDF](#)
- Jones DF, Treloar LRG (1975) The properties of rubber in pure homogeneous strain. *J Phys D Appl Phys* 8:1285–1304
- Lari DR, Schultz DS, Wang AS, On-Tat L, Stewart JM (2012) Scleral mechanics: comparing whole globe inflation and uniaxial testing. *Exp Eye Res* 94:128–135 [PDF](#)
- Mangan R, Destrade M (2015) Gent models for the inflation of spherical balloons. *Int J Non-Linear Mech* 68:52–58 [PDF](#)
- Mansouri MR, Darijani H (2014) Constitutive modeling of isotropic hyperelastic materials in an exponential framework using a self-contained approach. *Int J Solids Struct* 51:4316–4326
- Meunier L, Chagnon G, Favier D, Orgéas L, Vacher P (2008) Mechanical experimental characterisation and numerical modelling of an unfilled silicone rubber. *Polym Test* 27(6):765–777
- Miehe C, Lulei F (2001) A physically-based constitutive model for the finite viscoelastic deformations in rubbery polymers based on a directly evaluated micro–macro-transition. In: Besdo D, Schuster RH, Ihlemann J eds. *Constitutive Models for Rubber II*, Taylor & Francis, 117–128
- Mooney M (1940) A theory of large elastic deformation. *J Appl Phys* 11:582–591
- Nah C, Lee GB, Lim JY, SenGupta R, Gent AN (2010) Problems in determining the elastic strain energy function for rubber. *Int J Non-Linear Mech* 45:232–235
- Ogden RW (1972a) Large deformation isotropic elasticity—on the correlation of theory and experiment for incompressible rubberlike solids. *Proc R Soc Lond A* 326:565–584
- Ogden RW (1972b) Large deformation isotropic elasticity—on the correlation of theory and experiment for compressible rubberlike solids. *Proc R Soc Lond A* 328:567–583
- Ogden RW (1984) *Non-linear elastic deformations*. John Wiley and Sons, New York
- Ogden RW, Saccomandi G, Sgura I (2004) Fitting hyperelastic models to experimental data. *Comput Mech* 34:484–502
- Omnès B, Thuillier S, Pilvin P, Grohens Y, Gillet S (2008) Effective properties of carbon black filled natural rubber: experiments and modeling. *Composites Part A: App Sci Manufacturing* 39(7):1141–1149
- Osborne WA (1909) The elasticity of rubber balloons and hollow viscera. *Proc R Soc Lond B* 81:485–499
- Penn RW (1970) Volume changes accompanying the extension of rubber. *Trans Soc Rheol* 14(4):509–517
- Poynting JH (1913) The changes in the length and volume of an India-rubber cord when twisted. *India-Rubber J* (4):6–7 (cited in Truesdell and Noll 1992, pp. 176, 235, 237 and 546)
- Richter H (1952) Zur elastizitätstheorie endlicher verformungen. *Math Nachr* 8:65–73
- Rivlin RS (1948) Large elastic deformations of isotropic materials IV. Further developments of the general theory. *Phil Trans R Soc Lond A* 241:379–397
- Sawyers K (1986) Comments on the paper *Determination of the stretch and rotation in the polar decomposition of the deformation gradient* by A. Hoger and D. E. Carlson. *Q J Appl Math* 44:309–311 [PDF](#)
- Steimann P, Hossain M, Possart G (2012) Hyperelastic models for rubber-like materials: consistent tangent operators and suitability for Treloar’s data. *Arch Appl Mech* 82(9):1183–1217 [PDF](#)
- Ting TCT (1985) Determination of $C^{1/2}$, $C^{-1/2}$ and more general isotropic tensor functions of C . *J Elast* 15:319–323
- Treloar LRG (1943) The elasticity of a network of long-chain molecules—II. *Trans Faraday Soc* 39:241–246
- Treloar LRG (1944) Stress-strain data for vulcanised rubber under various types of deformation. *Trans Faraday Soc* 40:59–70
- Treloar L (2009) *The physics of rubber elasticity*, 3rd edn. Clarendon Press, Oxford
- Truesdell C (ed) (1965) *Continuum mechanics III, foundations of elasticity theory*. Gordon and Breach, New York a parenthetical comment of the reference Richter H (1952)
- Truesdell C (1984) *Rational thermodynamics*. Springer, New York
- Truesdell C, Noll W (1992) *The nonlinear field theories of mechanics*, 2nd edn. Springer, New York
- Urayama K (2006) An experimentalist’s view of the physics of rubber elasticity. *J Polym Sci B Polym Phys* 44(24):3440–3444
- Valanis KC, Landel RF (1967) The strain-energy function of a hyperelastic material in terms of the extension ratios. *J Appl Phys* 38:2997–3002
- VanArsdale WE (2003) Objective spin and the Rivlin–Ericksen model. *Acta Mech* 162:111–124
- Varga OH (1966) *Stress–strain behavior of elastic materials*. John Wiley and Sons, New York
- Yeoh OH (1990) Characterization of elastic properties of carbon-black-filled rubber vulcanizates. *Rubber Chem Technol* 63(5):792–805
- Yeoh OH, Fleming PD (1997) A new attempt to reconcile the statistical and phenomenological theories of rubber elasticity. *J Polym Sci B Polym Phys Ed* 35(12):1919–1932

Publisher’s note Springer Nature remains neutral with regard to jurisdictional claims in published maps and institutional affiliations.